Supplemental Information for: Velocity-Dependent Dynamics of Friction and Wear

Even Marius Nordhagen, Henrik Andersen Sveinsson, Anders Malthe-Sørenssen

S1 Asperity trajectory

During sliding, the asperity travels 3 units in the x- direction for every 1 unit in the y direction ($v = (3, 1)v$), inspired by Ref. [1]. The asperity starts at position $r_0 = (L/2, 2L/3)$ and moves until it hits position $r_1 = (L/2, L/3)$, see Fig. S1. The total length travelled is thus $\Delta x = 2L$ in x-direction and $\Delta y = 2L/3$ in y-direction. With $L = 20$ nm, the total sliding distance of the asperity is

$$\Delta r = \sqrt{\Delta x^2 + \Delta y^2} = 2L\sqrt{\frac{10}{9}} \approx 42.1\,\text{nm}. \tag{S1}$$

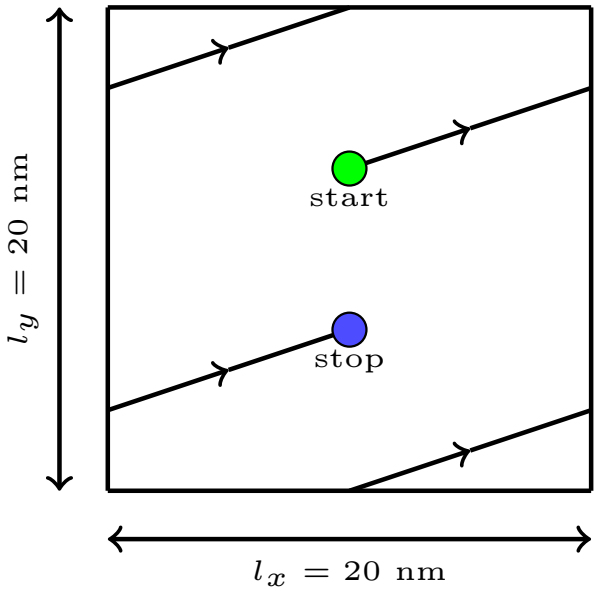

Figure S1: Asperity trajectory on the xy-plane. The green dot ($L/2$, $2L/3$) is the starting point of the asperity, while the blue dot ($L/2$, $L/3$) is the endig point

S2 Cylindrical asperity

In order to ascertain that the non-monotonic frictional behavior is not exclusively attributed to the particular geometry of the asperity, we conducted additional simulations of a cylindrical asperity. Since a cylinder is far from the Wulff shape of silicon carbide [2], these simulations were only viable at low temperature ($T = 1200$ K). The initial contact area of the cylindrical asperity was chosen to match the initial contact area of the original asperity. The cylindrical asperity is here denoted by "cylinder" while the original asperity is denoted by "pyramid" due to its inverted shape. Figure S2 compares friction and wear of the two asperities. We observe that the cylindrical asperity also has a non-monotonic velocity dependency on friction (Fig. S2), although not as distinct as for our original asperity. A non-monotonic velocity dependency on wear is not obvious for the cylindrical asperity.

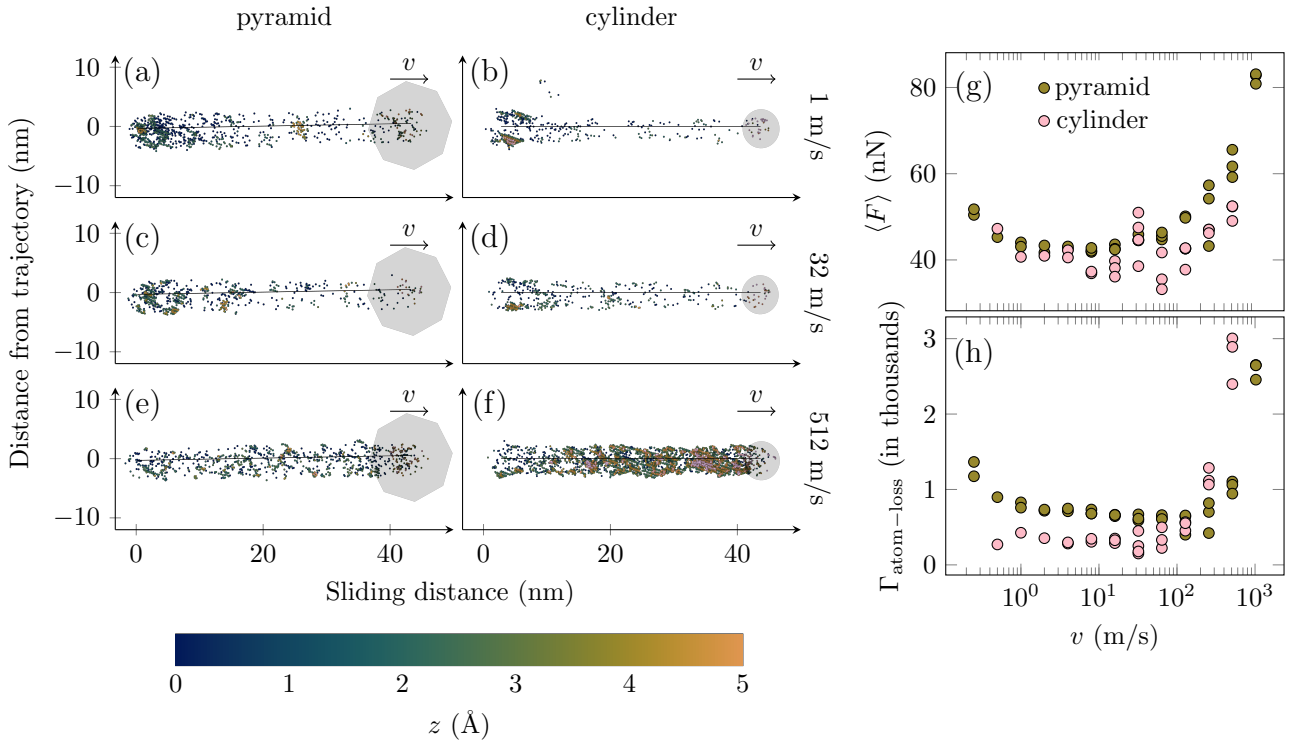

Figure S2: Friction and wear for a cylindrical (cylinder) and our original asperity (pyramid) at $T = 1200$ K. (a)-(f) displays the asperity residual films at selected velocities (1, 32 and 512 m/s). (g) illustrates the average friction as a function of velocity with a logarithmic x-scale. (h) shows the atom loss as a function of velocity with a logarithmic x-scale. (g) and (h) share labels.

S3 Predicted lateral force

Figure S3 illustrates the time-dependent model of static friction in Eq. 4 in the main text and compare it to the average static friction (Eq. 6) for various velocities. Only one temperature (1200 K) is displayed, but the shape of the friction curves are equivalent for different temperatures, but with different sawtooth amplitudes.

To estimate the average static friction, we evaluate the integral numerically. We do this by including ten sawtooth peaks, just like in the Fig. S3. Here it is important to choose a sufficient number of sampling point, given by the Nyquist sampling rate – a too small number of sampling points will cause aliasing and might greatly affect the estimate of the integral.

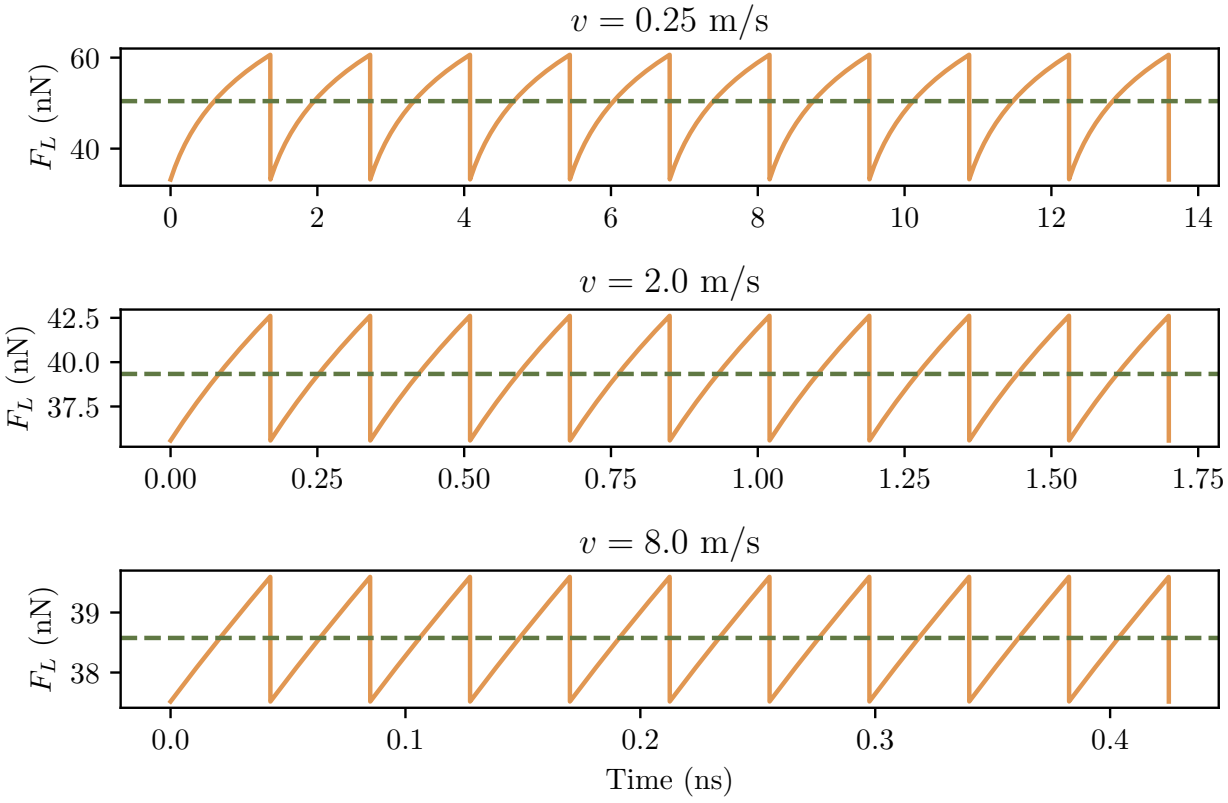

Figure S3: Lateral force as a function of time, modeled by Eq. 4 in the main text with the obtained parameters. Velocities are 0.5, 2 and 8 m/s seen from top. Temperature 1800 K.

S4 Contact time

The contact age during the sticking phase of stick-slip sliding determines the rate of the velocity-weakening effect. We measure the contact age as the time between a prominent local minimum and a following prominent local maximum, as shown in the first column of Figs. S4 and S5. Similarly, the contact stiffness was measured as the slope of a sawtooth with respect to the sliding distance ($k = \Delta F/\Delta x$). Contact time distributions are shown in second column of Figs. S4 and S5 and stiffness distributions are shown in third column of Figs. S4 and S5.

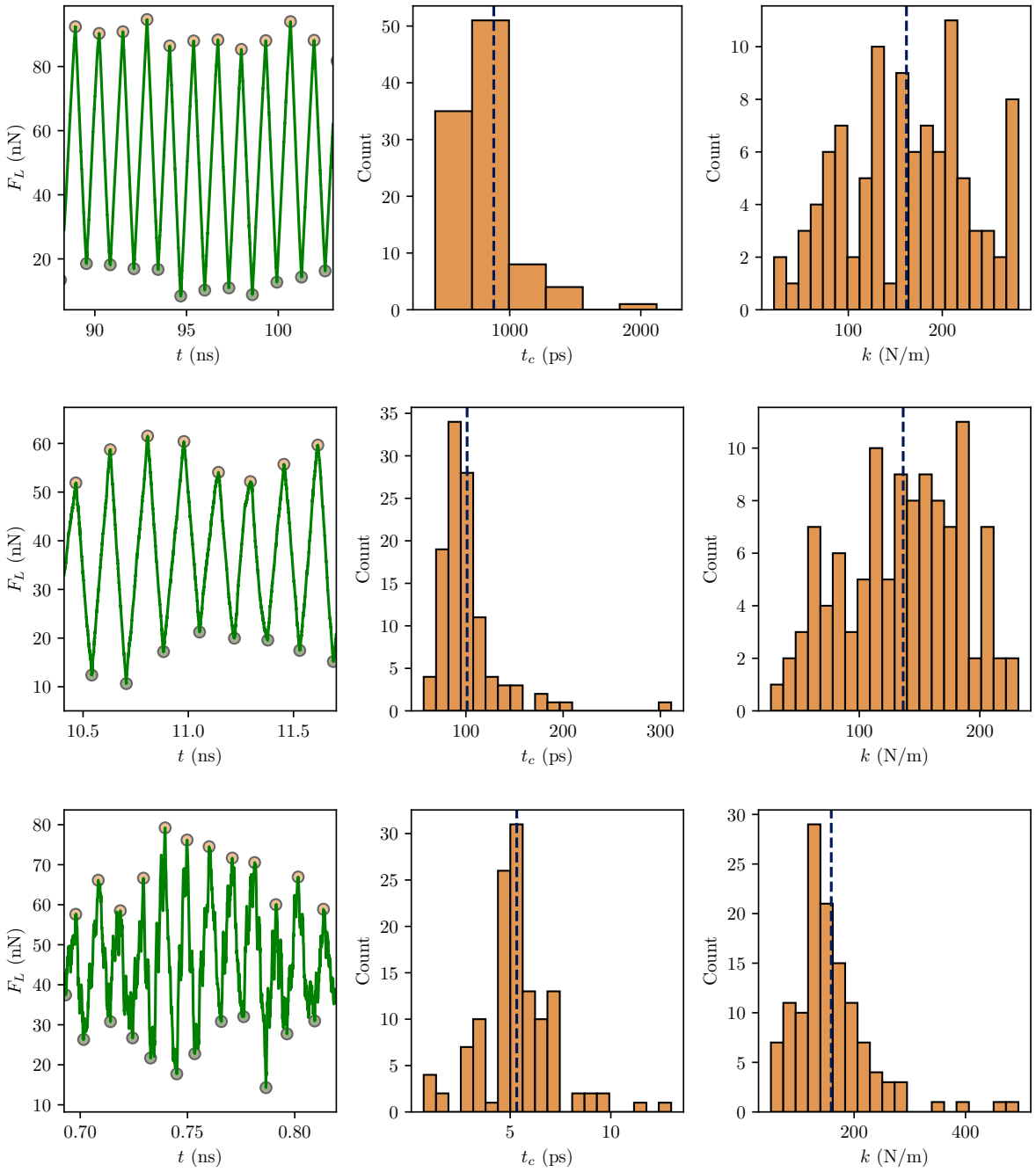

Figure S4: Contact time and asperity stiffness during stick-slip sliding. First column presents the strategy of contact time measurements. Second column displays the contact time distribution with dashed line indicating the average contact time. Third column displays the stiffness distribution, with dashed line indicating the average stiffness. The the three rows correspond to $T = 1200$ K and $v = 0.25$ m/s, $v = 3$ m/s and $v = 32$ m/s seen from top.

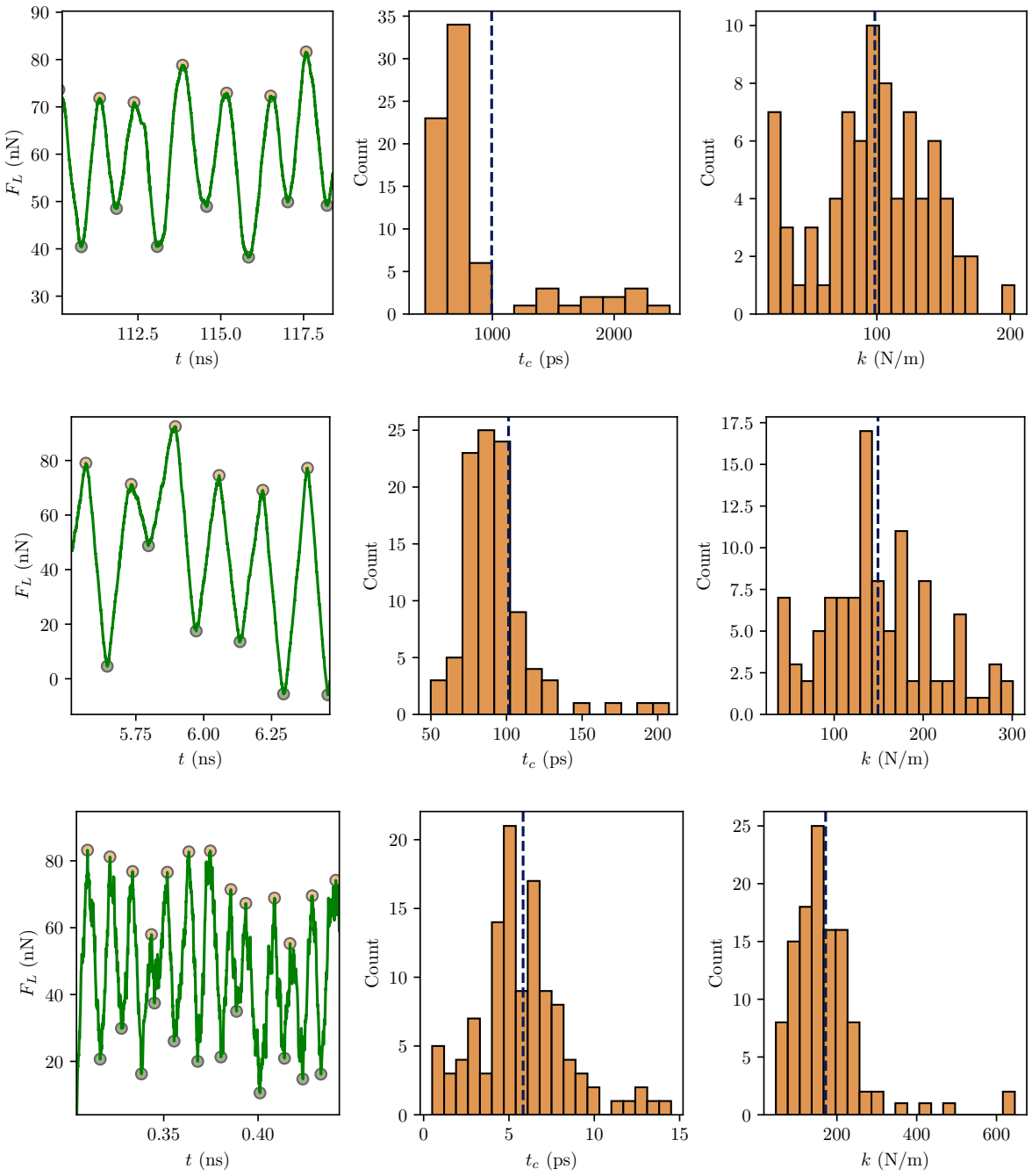

Figure S5: Contact time and asperity stiffness during stick-slip sliding. First column presents the strategy of contact time measurements. Second column displays the contact time distribution with dashed line indicating the average contact time. Third column displays the stiffness distribution, with dashed line indicating the average stiffness. The the three rows correspond to $T = 2300$ K and $v = 0.25$ m/s, $v = 3$ m/s and $v = 32$ m/s seen from top.

For immediate slips, the average contact time corresponds to the theoretical upper bound $\langle t_c \rangle = a/v$. In Fig. S6, the average contact age for various temperatures is plotted as a function of velocity with the theoretical upper bound for $a = 0.34$ nm. The theoretical upper bound is a observed to be a good estimate.

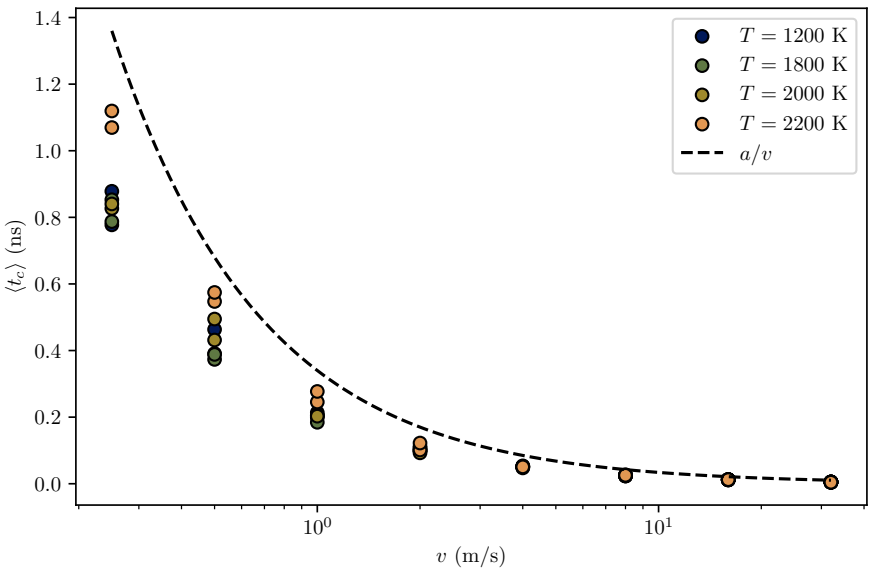

Figure S6: Average contact time as a function of velocity with a logarithmic x-scale. The dashed line corresponds to the theoretical upper bound contact time.

S5 Frictional aging

Here, we estimate the aging parameters f, U_{attr} and Ω by examining the contact area growth of a single asperity. We perform molecular dynamics simulations at various temperatures in the relevant regime ($T \in \{1800, 2000, 2200\}$ K) over 20 ns where the real contact area is measured every 100 ps. The system is equivalent to the one described in the main text, and the simulation procedure follows the one described in Ref. [3]. To obtain the aging parameters, we fit the contact area change to the aging model in Eq. 5 in Ref. [3]:

$$A(t) - A(0) = c\frac{k_{\text{B}}T}{\Omega} \log\left(1 + \frac{\Omega t}{k_{\text{B}}T} f \exp\left(-\frac{U_0}{k_{\text{B}}T},\right)\right). \tag{S2}$$

Here, $A(0)$ is the initial contact area, c is the proportionality constant between the number of facets and contact area, Ω is the rate of the energy barrier, k_{B} is the Boltzmann constant, T is the temperature and U_0 is the initial energy barrier. The contact area as a function of contact age and a model fit is plotted in Fig. S7.

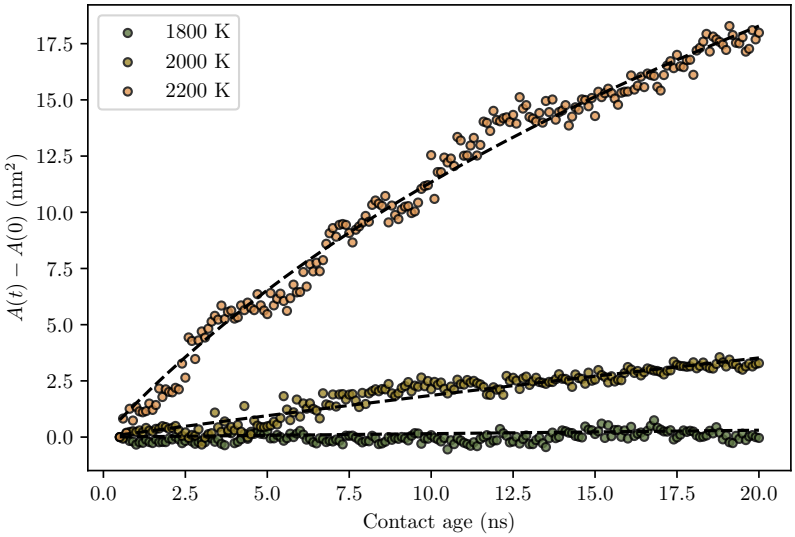

Figure S7: Contact area evolution for various temperatures.

The model fit utilizes that the contact interface is close to square-shaped, such that the relation $c = 4\sqrt{2}sd$ can be applied. Here, $s = 5.6$ nm is the initial width of the contact interface and $d = 0.31$ nm is the thickness of a facet layer. The obtained values from the fit are $f = 1.7 \times 10^8$ ns^{-1}, $U_{\text{attr}} = 3.9$ eV and $\Omega = 0.10$ eV. Note that in the original paper (Ref. [3]) the asperity and the substrate had matching crystal lattices contrary to here, resulting in stronger frictional aging.

S6 Shear wave speed

The shear wave speed in our crystal was obtained through the expression

$$c_s = \sqrt{\frac{G}{\rho}}, \tag{S3}$$

where G is the shear modulus and ρ is the material density. The shear modulus and density were measured at various temperatures ($T \in [1000, 2200]$ K) through molecular dynamics simulations as described in Ref. [4] (note that the shear modulus corresponds to the elastic constant c_{55} in Voigt notation). All three quantities (G, ρ and c_s) exploit linearly decreasing dependencies on temperature within our temperature regime (Figure S8).

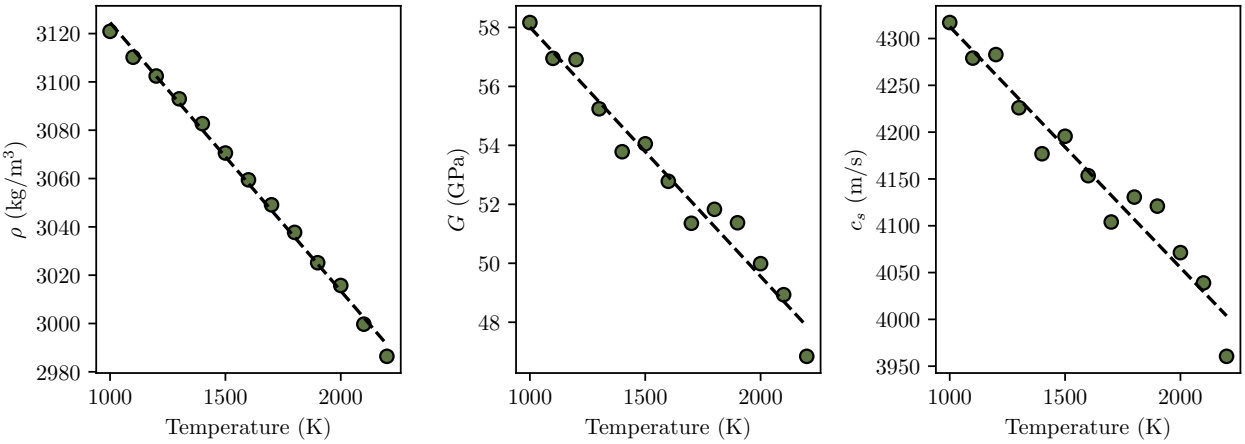

Figure S8: Material density (left), shear modulus (middle) and shear wave speed (right) as a function of temperature.

S7 Wear versus friction

Here we investigate how wear depends on the frictional force (Fig. S9). We observe that wear is not a unique function of friction. Instead, wear is larger per friction at low velocities. The friction-wear relationship becomes more similar for the low and high velocity regimes as the temperature increases.

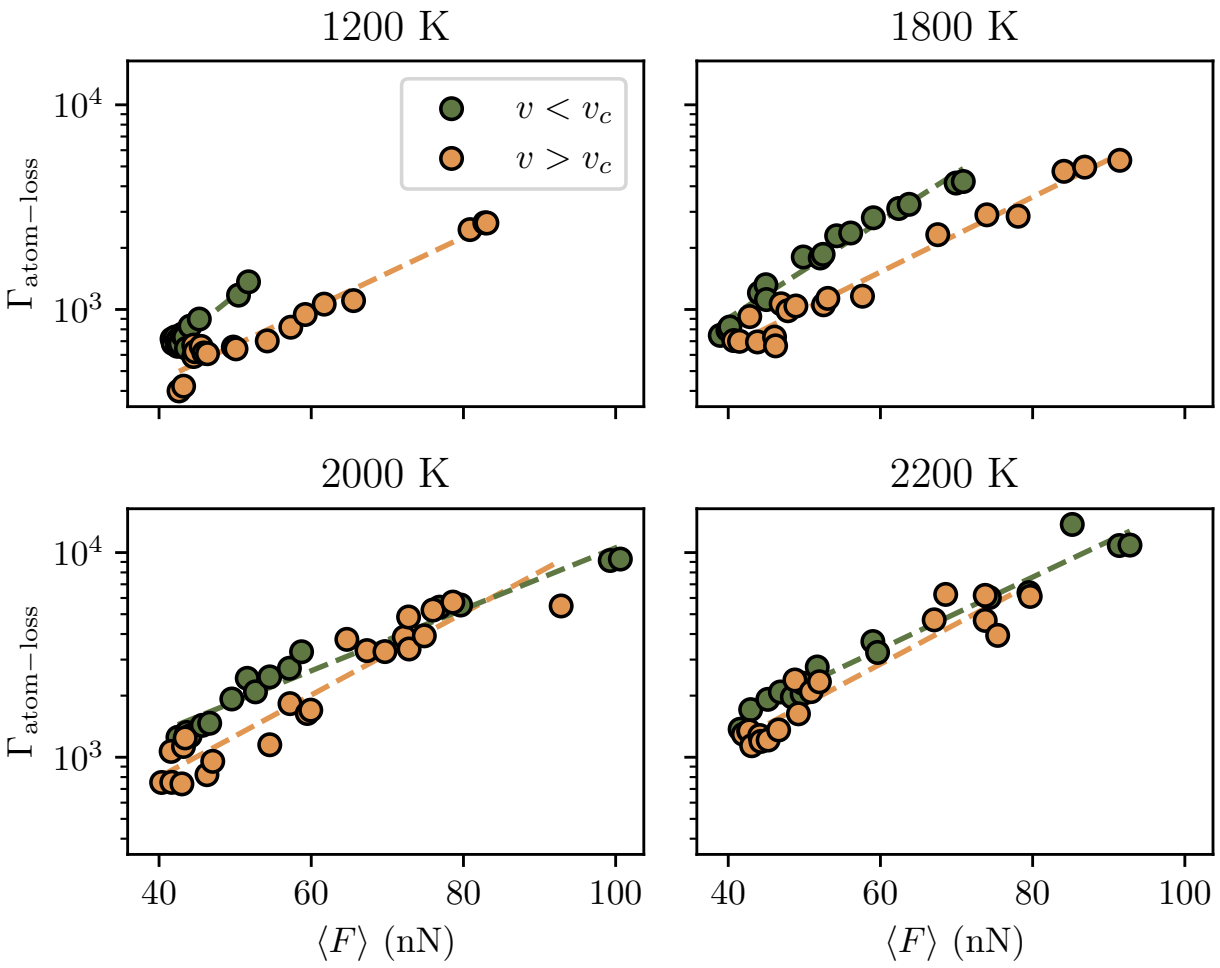

Figure S9: Wear as a function of friction for various temperatures $T \in \{1200, 1800, 2000, 2200\}$ K. Green points are points at low sliding velocity $v < v_c$, while orange points corresponds to high sliding velocities $v > v_c$. Linear fits are done separately for the low and high velocity regimes and also separately for the various temperatures.

References

1. Schall, J. D., Milne, Z. B., Carpick, R. W. & Harrison, J. A. Molecular Dynamics Examination of Sliding History-Dependent Adhesion in Si–Si Nanocontacts: Connecting Friction, Wear, Bond Formation, and Interfacial Adhesion. *Tribol. Lett.* **69,** 52 (2021).
2. Sveinsson, H. A. *et al.* Direct Atomic Simulations of Facet Formation and Equilibrium Shapes of SiC Nanoparticles. *Cryst. Growth Des.* **20,** 2147–2152 (2020).
3. Nordhagen, E. M., Sveinsson, H. A. & Malthe-Sørenssen, A. Diffusion-Driven Frictional Aging in Silicon Carbide. *Tribol. Lett.* **71,** 95 (2023).
4. Guren, M. G., Sveinsson, H. A., Malthe-Sørenssen, A. & Renard, F. Nanoscale Damage Production by Dynamic Tensile Rupture in alpha-Quartz. *Geophysical Research Letters* **49,** e2022GL100468 (2022).